J. Fluid Mech. (1974), *vol.* 66, *part* 2, *pp.* 223–239
Printed in Great Britain

Experimental study of internal waves over a slope

By DAVID CACCHIONE

Office of Naval Research, 495 Summer Street, Boston, Massachusetts 02210

AND CARL WUNSCH

Department of Earth and Planetary Sciences, Massachusetts Institute of Technology, Cambridge

(Received 25 January 1974)

Internal waves of the fundamental mode propagating into a shoaling region have been studied experimentally in a continuously stratified fluid. The waves divide into three classes depending upon the ratio of the bottom slope γ to the wave-characteristic slope c. For $\gamma/c < 1$, the amplitude and wavenumber changes of the waves over the slope are in reasonable accord with a simple inviscid linear theory, prior to wave breakdown near the intersection of the slope and surface. Considerable mixing occurs in this corner region. When $\gamma/c = 1$, a striking instability of the bottom boundary layer is observed and the waves are heavily damped. When $\gamma/c > 1$, the waves are inhomogeneous and have complex spatial dependence.

1. Introduction

Considerable effort has been made towards a theoretical understanding of the interaction of internal waves and topographic features. Major attention has been given to the linear problem of internal wave propagation over regions of variable bottom topography (Sandstrom 1966; Magaard 1962; Wunsch 1969; Keller & Mow 1969; Baines 1971; and others). The problem not only presents some unusual mathematical difficulties, but in addition has geophysical applications of considerable interest. For example, the linear theories (e.g. Sandstrom 1966; Wunsch 1969) all predict that if the bottom slope is sufficiently small (defined explicitly below) internal wave energy will accumulate at the intersection of the sea bottom with the top of the stratified layer. Continental margin areas often represent such a situation, and there may be a significant effect on the mean oceanic conditions in these boundary areas where incident internal wave energy is dissipated. The linear theories also predict that, near a particular frequency, the motion induced along the sea floor becomes very large, and there is a possibility, discussed by Cacchione & Southard (1974), that sediment may be moved by shoaling internal waves.

The details of the boundary layer induced along the bottom have been examined by Wunsch (1969), Wunsch & Hendry (1972), and in a somewhat indirect fashion by Hart (1971). In addition to these linear problems, it has been shown by Wunsch (1971) and Hogg (1971) that Reynolds stress effects of shoaling

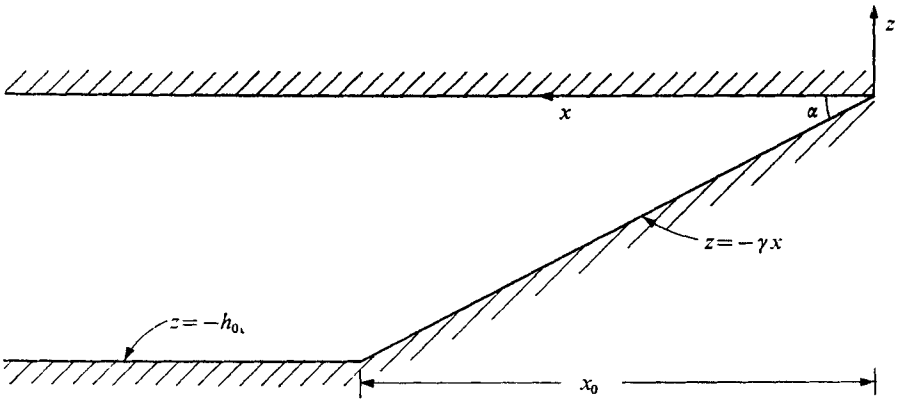

FIGURE 1. Geometry and co-ordinate system of the theoretical solutions. The theory does not take explicit account of the 'transition corner' occurring at $x = x_0$.

internal waves may be able to deform the mean density field, and even drive long-shore ('long-slope') mean currents. These effects have never been demonstrated in the ocean.

In this paper we describe the results of a series of laboratory experiments intended to test some of the simpler ideas that emerge from the linear theories for internal wave propagation over a sloping bottom. A previous crude experiment related to this work was described by Wunsch (1969). The present experimental results show some especially striking features in the bottom boundary layer.

2. Theoretical background

The analytic theory of internal waves propagating over a linear sloping bottom described by Wunsch (1969), hereafter denoted as I, is formally the simplest of the solutions alluded to above. For this reason the experiments were designed with this theory as a guide, though the work presented here is primarily experimental, and we have not attempted an extension of the theory to account for the physical details.

We confine our attention to small amplitude two-dimensional waves propagating in a fluid having constant buoyancy (Brunt–Väisälä) frequency N over a planar bottom slope as shown in figure 1. The vertical co-ordinate z is positive upwards; the horizontal co-ordinate x increases in the direction of increasing water depth. (We shall hereafter refer to the point $x = z = 0$ as the 'corner'.) The water depth is $z = -\gamma x$. Let σ be the wave frequency and define a stream function such that

$$u = -\partial\psi/\partial z, \quad w = \partial\psi/\partial x,$$

where u and w are in the conventional x and z directions. The fluid surface is assumed to be rigid. Wunsch (1969) shows that, if we define $c^2 = \sigma^2/(N^2 - \sigma^2)$, then

$$\frac{\partial^2\psi}{\partial z^2} - \frac{1}{c^2}\frac{\partial^2\psi}{\partial x^2} = 0. \tag{1}$$

The inviscid linear solutions to (1) fall into three classes: (i) $\gamma < c$, 'subcritical' or 'transmissive' slope, representing waves with phase and group velocity

everywhere in the direction of shoaling water; (ii) $\gamma > c$, 'supercritical' or 'reflective' slope, for which all incident wave energy is reflected back into the interior; (iii) $\gamma = c$, 'critical' slope, for which the direction of energy propagation is parallel to the bottom slope. The reflexion properties of the slope can be inferred most directly from the reflexion conditions deduced by Phillips (1966). Note that c is the slope of the characteristics of the hyperbolic equation (1) along which wave energy propagates.

For class (i) the solutions given in I for waves travelling towards the corner are

$$\left.\begin{aligned} \psi(x,z) &= A\{\exp[-iq\ln(cx-z)]-\exp[-iq\ln(cx+z)]\}, \\ q &= 2n\pi/\ln\Delta, \quad \Delta = (c+\gamma)/(c-\gamma), \quad n = 1,2,\ldots. \end{aligned}\right\} \tag{2}$$

A strong amplification is predicted along the bottom slope, and the wave energy propagates into the corner. Greenspan (1969) demonstrates that, as long as linear theory is valid, the group velocity of the incident waves decreases with the water depth in such a way that the travel time into the corner is infinite. As far as the class (i) linear solutions are concerned, the container is 'open' (cf. Beardsley 1970). In practice of course, nonlinearities or viscous effects must become important to prevent the infinity in the energy density in the corner. It was also shown in I that, for sufficiently small values of γ/c and far from the corner ($x \gg z/c$), the horizontal wavelength implicit in (2) is asymptotically the same as the wavelength predicted over a flat bottom (Lamb 1932, p. 379). Keller & Mow (1969) obtained the same result from a geometrical optics argument.

When $\gamma > c$ the solutions in (2) are formally valid but have a singularity present in the interior of the fluid along the line $z = -cx$ emanating from the corner. Solutions in which this singularity was removed are also presented in I. Energy impinging on the slope is reflected backwards into deeper water in this case. (See also the discussion by Robinson 1970.)

Equation (2) is singular as $\gamma \to c$; infinite velocities are predicted along the slope. When $\gamma = c$ the singularity at $z = -\gamma x$ cannot be removed within the inviscid small amplitude theory.

The Schmidt number for the salt solutions used in the experiments is about 10^3, and we shall assume that for discussion purposes the boundary layers for infinite Schmidt number given in I are adequate. In I it is shown that for $\gamma \neq c$ the boundary layer along the bottom slope is essentially a Stokes oscillating boundary layer for which the non-dimensional boundary-layer thickness is

$$\frac{R^{-\frac{1}{2}}}{\sqrt{2}}\left(\frac{\sigma}{N}\right)^{\frac{1}{2}}\left(\frac{\sigma^2}{N^2-\sin^2\alpha}\right)^{-\frac{1}{2}} = L^{-1}\left(\frac{\nu}{2\sigma}\right)^{\frac{1}{2}}\left(1-\frac{N^2}{\sigma^2\sin^2\alpha}\right)^{-\frac{1}{2}}.$$

(R is a Reynolds number defined as $R = NL^2/\nu$, where ν is molecular viscosity, L is the local water depth and $\gamma = \tan\alpha$.) The dimensional thickness was about 0·3 cm in the experiment. When $\sigma^2/N^2 - \sin^2\alpha < O(R^{-\frac{1}{2}})$, i.e. $\gamma \approx c$, the boundary layer formally has non-dimensional thickness $R^{-\frac{1}{2}}$. But as we shall see below, the experimental results show that for $\gamma \approx c$ the boundary layer exhibits a striking instability. At the order of approximation of I, no dissipation of the interior wave field takes place.

Phillips (1970) and Wunsch (1970) have shown that an additional buoyancy

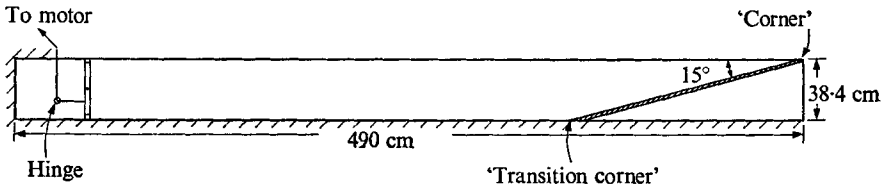

FIGURE 2. The wave tank, showing the position of a 15° slope. The paddle was connected through linkages to a driving motor.

boundary layer exists along the sloping boundary in a stratified fluid. A slow mean flow is driven up the slope over a boundary-layer thickness of order

$$(\nu\kappa)^{\frac{1}{4}}/(N\sin\alpha)^{\frac{1}{2}},$$

where ν and κ are the diffusivities of momentum and salt, respectively. In the geometry shown in figure 1 and with $\nu = 10^{-2}\,\mathrm{cm}^2/\mathrm{s}$ and $\kappa = 10^{-3}\,\mathrm{cm}^2/\mathrm{s}$, this boundary-layer thickness is of order 0·05 cm and may be ignored in the discussion of the wave-driven boundary layer.

3. Experimental arrangement

3.1. *Geometry*

The basic geometry of the experimental set-up is shown in figure 2, and differs from the geometry of the above theoretical discussion in two major ways. First, a free surface was used over the slope, instead of a rigid upper lid. Phillips (1966) shows that at small wavelengths this difference has negligible effects on the wave motion. In the experiments, vertical motion of the free surface was almost undetectable and is not thought to have influenced significantly the internal motion over the sloping bottom. Of course, the structure of the upper surface boundary layer (a Stokes layer) is slightly different for a rigid top, but this change is of no consequence in the results.

Second, the wave motion was generated by a paddle in a region of constant depth and a finite distance from the sloping bottom, leading to a 'transition corner' region, depicted in figure 2, at a distance x_0 from the origin at the apex. Robinson (1970) has considered the effects of such a corner in detail, by discussing the diffractive contributions to the ordinary ray solution (which is asymptotically equal to equation (2) as the distance from the transition corner increases). His conclusion is that the ray solution is quantitatively correct as one departs from the ray ($z - cx =$ constant) emanating from the corner itself. In the immediate vicinity of this ray, he shows that linear theory breaks down, non-linearity smooths out the singularity in the linear solution and, in addition, diffractive effects occur at the corner. Anticipating the results of the experiments, we did not detect any singularities associated with this corner.

3.2. *Apparatus*

A glass rectangular wave tank 4·9 m long, 21 cm wide and 38 cm deep was filled with a salt-stratified water solution using a technique similar to that described by Oster (1965). The range of density gradients selected corresponded to

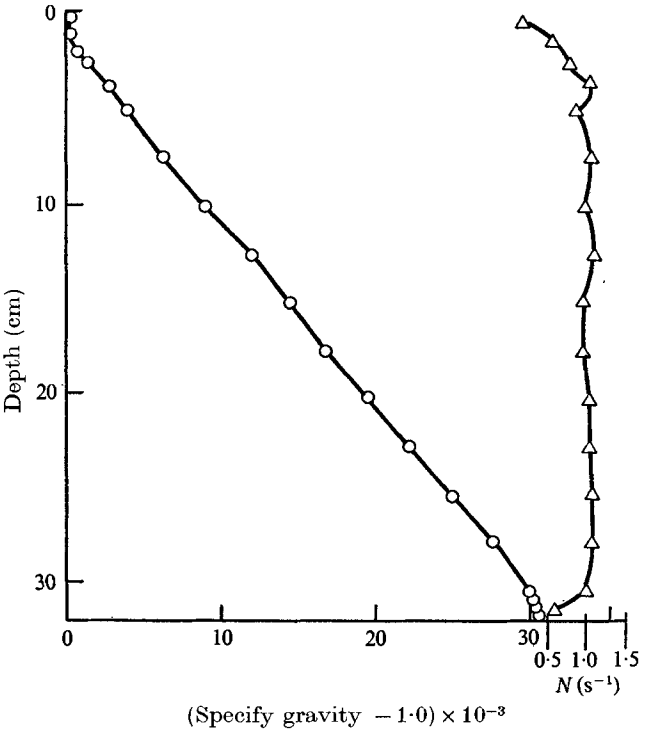

FIGURE 3. Specific gravity and buoyancy frequency N in a typical experimental run. ○, specific-gravity measurements; △, buoyancy-frequency values N computed from the specific-gravity profile. 'Tails' at top and bottom are due to boundary conditions.

buoyancy frequencies N between $0{\cdot}6\,\mathrm{s}^{-1}$ and $1{\cdot}0\,\mathrm{s}^{-1}$. Density profiles like that shown in figure 3 were obtained by determining the index of refraction of samples of small volume (< 1 ml) with a hand-held refractometer. The index of refraction was converted directly to density by applying a calibration technique that included a correction for local temperature measured with a thermistor.

Nonlinear tails in the density gradients normally formed near the bottom and below the free surface (cf. Mowbray 1967). Evaporative cooling, when the flexible plastic cover was removed from the slope section during the measurements, resulted in a more homogeneous layer at the free surface. Evaporation was reduced significantly (to less than 1 mm/day) when a plastic cover was in place.

A paddle capable of generating the first-mode internal wave was placed at the far end of the tank (figure 2). The paddle was hinged at its mid-point and driven by a variable-amplitude scotch yoke connected to a variable-speed drive on a $\frac{1}{4}$ h.p. motor. Frequencies could be selected in a continuous band over the entire range of internal wave frequencies (up to $1{\cdot}5\,\mathrm{s}^{-1}$). Rubber gaskets sealed the edges of the paddle. That the fundamental mode was indeed being generated was checked by streak photographs and through the dispersion relation. Extraneous modes appear to have represented only a few per cent of the energy emanating from the paddle.

Time series of conductivity fluctuations at selected points in the tank were used to measure the internal wave motion. Over the range of salinity values used

during this study, salinity is approximately proportional to conductivity. The temperature variations in the water were small (usually less than 0·3 °C over the total depth) except in the upper 2 cm, so that the total change in conductivity at a point below the upper few centimetres is a valid estimate of the total change of salinity. The conductivity probes and associated circuitry used to make the measurements are described by Cacchione (1970).

Six data channels were sampled sequentially once per second and recorded on magnetic tape. Normally, voltage signals from four conductivity probes, the potentiometer circuit on the wave maker and a stable constant reference voltage were recorded. *In situ* calibration of each probe was accomplished during each experiment by raising and lowering the probe over several 1 mm depth increments and logging voltage *vs.* position.

Periodogram estimates were computed from the conductivity and wavemaker records. The starting point on each data record for periodogram computation was selected when it had been determined that the wave motion was well established. Calibration constants were then applied to the periodogram amplitudes a_m to yield the wave amplitude in cm at each probe location.

The periodogram estimates were usually normalized by similar estimates a_0 obtained from conductivity data taken over the flat-bottom regions during the same experimental run and at the same depth by the same probe. The results are in the form a_m/a_0 and are a measure of the change in wave amplitude from the flat bottom to the slope taken by each probe. This normalization conveniently removes certain calibration constants, and provides a non-dimensional expression that can be compared with an equivalent theoretical estimate.

The phase values θ for closely spaced adjacent probes at the same depth were used to determine experimental values of the horizontal wavenumber k_E from the expression

$$k_E \approx \Delta\theta/\Delta x \quad \text{for} \quad \Delta x \ll \lambda,$$

where $\Delta\theta = \theta_{i+1} - \theta_i$, $\Delta x = x_{i+1} - x_i$ and λ is the horizontal wavenumber. (i denotes an arbitrary probe location in the tank, and $i+1$ that of the adjacent probe.) Record durations of at least 50 wave periods, often up to 100, were obtained for quasi-steady conditions.

4. Results

The results are separated into three basic categories: (i) one that describes the interior wave field (wavenumber and wave amplitude); (ii) another that describes the activity at the boundaries; and (iii) a discussion of wave breakdown. Considerably more detail about the results may be found in Cacchione (1970).

Since N and γ were constant during each experiment, the ratio γ/c could be altered by changing σ. In this way, all three hydrodynamic regimes $\gamma/c < 1$, $\gamma/c > 1$ and $\gamma/c = 1$ were investigated during each experiment.

4.1. *Interior wave field*: $\gamma < c$

Streak photographs of neutrally buoyant particles confirmed that the fundamental mode was indeed the dominant motion. The predicted bottom intensification could also be clearly seen in the photographs.

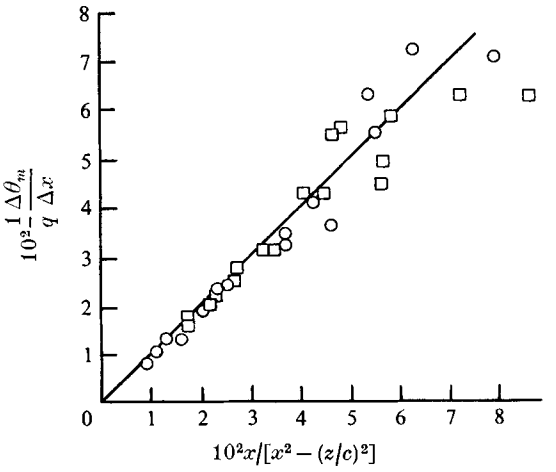

FIGURE 4. The experimental wavenumber plotted *vs.* its theoretical value for $\gamma < c$. In both cases shown, $a_0 = 0{\cdot}2$ cm. □, 'low' frequency waves in which $\sigma/N \simeq 0{\cdot}07$; ○, 'high' frequency waves with $\sigma/N \simeq 0{\cdot}13$. However, in both cases different runs had somewhat different frequencies. The corner is at the upper right. Data were taken at various values of z.

Wavenumber. An experimental wavenumber k_m was computed from the measured phase differences between adjacent probes. In figure 4 we plot k_m/q [q is defined in (2)] against its theoretical value $x/[x^2-(z/c)^2]$ over the slope, where the expression is averaged for the position of the two probes. Measurements are shown only in the region well away from the wave breakdown area and outside the bottom boundary layer, where the linear inviscid theory is presumably applicable.

The theoretical curve in figure 4 is a straight line with a slope of unity. Typical experiments with different frequencies and amplitudes are shown. The upper right portion of the diagram corresponds to the corner region ($x, z = 0$) of the slope. The plot shows that the wavenumber decreases with increasing distance from the corner. The agreement of the results with the theoretical curve is best for waves over the lower section of the slope, well away from the corner. Apparently, the transition corner region has little or no effect on the wave motion. Towards the corner, the data points depart significantly from the theoretical curve for the lower frequency waves where the predicted increase in wavenumber does not take place. There is also some evidence in other data of an amplitude dependence in the wavenumber variation. The experimentally determined value of the wave steepness $\epsilon = a_m k_m$ at the positions nearest the corner is approximately 0·15; nonlinear effects are apparently already beginning to have a significant effect on the motion.

Wave amplitude In figure 5 we show the measured *vs.* theoretical wave amplitude squared. We chose this form of representation since the measured wave displacement is a complicated function of position. Lower frequency waves, with $\sigma/N \simeq 0{\cdot}07$, show earlier departures from the theoretical curves than do the high frequency waves, with $\sigma/N \simeq 0{\cdot}13$. Actual amplitudes are much lower than those

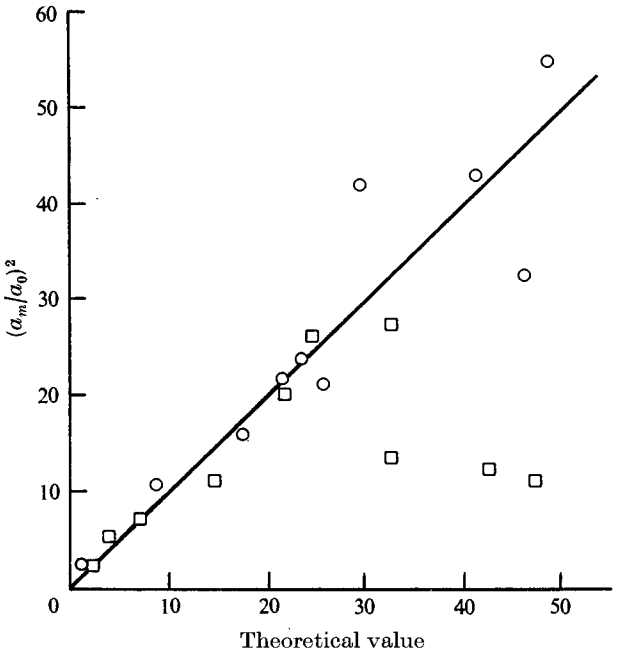

FIGURE 5. The measured square of the amplitude ratio *vs.* its theoretical value. ○, results for 'high' frequencies, $\sigma/N \simeq 0{\cdot}13$, which are in quite good agreement with the theory even at very large values; □, results for lower frequencies, $\sigma/N \simeq 0{\cdot}07$, which fail to attain the predicted high values, principally because of the strong dissipation along the slope. Data were taken at various values of z.

predicted on the middle and upper sections of the slope for the lower frequency waves. At these slope sections it was also found that the measured values of steepness are considerably less than those estimated from inviscid theory. The larger input waves ($a_0 = 0{\cdot}4$ cm) show a tendency to peak earlier than predicted.

Departure from theoretical estimates is most noticeable for the very low frequencies. Possibly a transformation from the sinusoidal wave form to a different wave structure (such as a solitary wave) that is heavily damped along the slope accounts for the nature of the experimental data for these kinds of waves (see below). In any event, the amplitude of these lower frequency waves is not as large as predicted, and there seems to be evidence of strong dissipation along the slope. The waves were observed to surge as they approach the corner.

4.2. *Boundary activity and breaking*: $\gamma < c$

These results are primarily qualitative. Observations of the oscillatory flow in the boundary layer and breaking zone were made with shadowgraph images, the motion of neutrally buoyant floats and dye streaks. One obvious major feature of this flow was its intensification near the bottom along the slope as compared with the flow along the horizontal bottom. The maximum velocities generally increased at positions further upslope, with a sharp growth in the velocities near

	L_b (cm)	
σ/N	$a_0 = 0{\cdot}2$	$a_0 = 0{\cdot}4$ cm
0·74	13·4	14·0
0·69	12·5	12·9
0·61	10·6	11·1
0·58	9·9	10·5
0·56	9·0	9·5
0·54	8·2	8·6
0·52	7·7	8·2

TABLE 1. Estimated position of breaking L_b measured along the slope from the corner $x = z = 0$.

the zone of breaking. The oscillatory flow remained laminar in the boundary layer up to the zone of breaking.

The breaking of waves on the relatively steep slopes (30 and 45°) is characterized by considerable turbulence and vertical motion below the free surface and by the generation of spatially irregular fine-structure in the density field. This kind of breaking is also observed for relatively high frequency waves on the smaller slopes (7 and 15°). In contrast, the lower frequency waves (i.e. those waves with frequencies closer to the condition $\gamma = c$) break much less violently, instead propagating upslope as distinctive bore-like features or 'surges' that eventually collapse and form a thin fluid stream along the slope, similar to the swash and backwash associated with the breaking of surface waves on a beach (see figure 6, plate 1). This phenomenon might also be related to the internal surf and swash described by Emery & Gunnerson (1973). Over larger slopes, the vortex breakdown is more violent.

For higher frequency waves, shortly after the first arrival of the waves near the top of the smaller slopes ($\alpha = 7$ and 15°), a small vortex forms along the slope beneath the crest of the advancing wave form. Figure 7 (plate 2) illustrates the onset of this instability beneath the wave crest. In the figure, the maximum amplitude of the incoming wave at the entrance to the slope region is approximately 0·4 cm. A similar phenomenon was noted by Thorpe (1966) (reproduced by Turner 1973, pl. XII). As the wave breakdown proceeds, one can see the protrusion of thin horizontal layers back into the interior region over the slope. The protrusions lose their intensity (as measured by photographic contrast) over very short horizontal distances (5–10 cm) and are confined to the upper vertical levels, where the breaking occurs. The protrusions, thin tongues of mixed fluid that are weakly convected back into the interior, are caused by mixing in the zone of breaking.

Table 1 presents a summary of shadowgraph observations of the positions L_b of breaking on slopes of 30°. L_b is measured from the corner along the slope. The accuracy of the distance L_b is low, owing to the difficulty in defining the point of breaking; however, the relative order of the values of L_b for the waves of different frequencies shown in the table is reliable. The general trend indicates that for a given N the higher frequency waves break first, i.e. in deeper water.

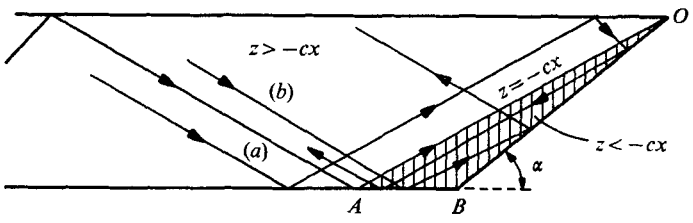

FIGURE 8. Detail of the reflexion characteristics for $\gamma > c$. Note the concentration of energy between the line $z = -cx$ and the slope (triangular area AOB).

4.3. *Interior wave field*: $\gamma > c$ *and* $\gamma = c$

For $\gamma > c$ (supercritical), two features are suggested by the theoretical reflexion properties: (i) the presence of back-reflected wave energy; (ii) concentration of this back-reflected energy in a zone bounded by the bottom slope and the characteristic that intersects the corner. Wave characteristics which are incident to the slope from above, i.e. those with a downward-pointing vertical energy component, upon reflexion from the slope will remain below the characteristic (defined by $z = -cx$) that intersects the corner (figure 8). The energy flux associated with these characteristics enters the slope region in a relatively broad band and leaves in a confined triangular zone, the triangular area AOB in figure 8. There is a smaller influx of energy which, upon reflexion from the flat bottom, propagates upslope within the narrow bottom zone (for example, the path of the characteristic (b) in triangle AOB). The characteristics associated with this latter energy flux have upward-pointing vertical components as they enter their slope regions; upon reflexion they preserve the sense of the upward-directed vertical components. In both cases (characteristics (a) and (b) in figure 8), once the characteristics reflect from the slope, the horizontal direction of energy propagation is away from the corner. The damping was sufficiently great that we could find no evidence for reflexion of energy from the paddle; some was undoubtedly present.

The theory of I selects $n = -2$ as the lowest non-singular inviscid mode permissible over the slope region for each of the experimental conditions tested. We had no means of generating this mode and hence could not make a direct experimental test of the reflective-mode solutions. For reference however, we plot the theoretical behaviour of the $n = -1$ solution (though it is singular along $z = -cx$) and the $n = -2$ solution in this regime.

In the experimental runs, the frequency of the wave at critical frequency was within 2 % of the required value.

Wavenumber. Figure 9 illustrates the complicated behaviour of the experimentally determined wavenumbers for $\gamma > c$. The calculated position of the critical characteristic (determined by $z = -cx$) for the experimental groups is shown along the horizontal axis. The theoretical curves were computed for two different values of the mode number.

There is a qualitative indication that the curves for $n = -1$ follow the same trend as the experimental results. The experimental values near the calculated singular lines are large, as expected; however, there is a significant shift in the

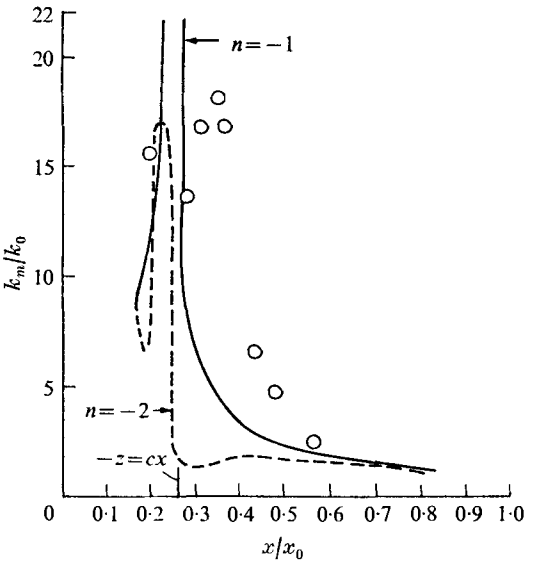

FIGURE 9. Spatial variation of the wavenumber for $\gamma > c$. $a_0 = 0{\cdot}2$ cm; $\sigma/N = 0{\cdot}05$. Also shown are the theoretical results for an $n = -1$ wave (which is singular) and an $n = -2$ wave (which is continuous). The wave generated corresponds to $n = -1$.

peak value to the right of the calculated critical point in figure 9. This shift probably indicates that the singularity is removed by nonlinear processes (as suggested by Robinson 1970) and, as expected, that the linear inviscid solutions are not valid here. The measured values of the steepness parameter ϵ for this particular data set are as large as 0·5 at $x/x_0 = 0{\cdot}36$. Nonlinear effects are probably significant near these positions.

Figure 10 summarizes the experimental results for the wavenumber for the critical case $\gamma = c$. The plot emphasizes the steep rise towards larger values of the wavenumber for decreasing distance to the corner. In general, the wavenumber variations with distance to the corner for this case are similar to the variations shown in figure 9 for the supercritical case.

In summary, the results show a complicated relationship between the wavenumber and position over the slope. There is evidence that the wavenumber increases rapidly as the waves pass over the lower and middle sections of the slope for the supercritical case. The variations in wavenumber for the critical case are qualitatively similar to those for the supercritical case. For both cases, the measured values of ϵ are greater than 0·1 for most of the measurements taken closest to the corner.

Wave amplitude. The results in figure 11 are presented as ratios of the square of the wave amplitude over the slope to the square of the wave amplitude over the flat bottom for various frequencies of the input waves. The horizontal axis, $-z/cx$, was chosen to facilitate interpretation of the results in terms of the reflexion properties of the slope. As described earlier, theory indicates that near the critical characteristic defined by $z = -cx$ and in a zone between this characteristic and the bottom slope (figure 8) there is a possible region of concentrated

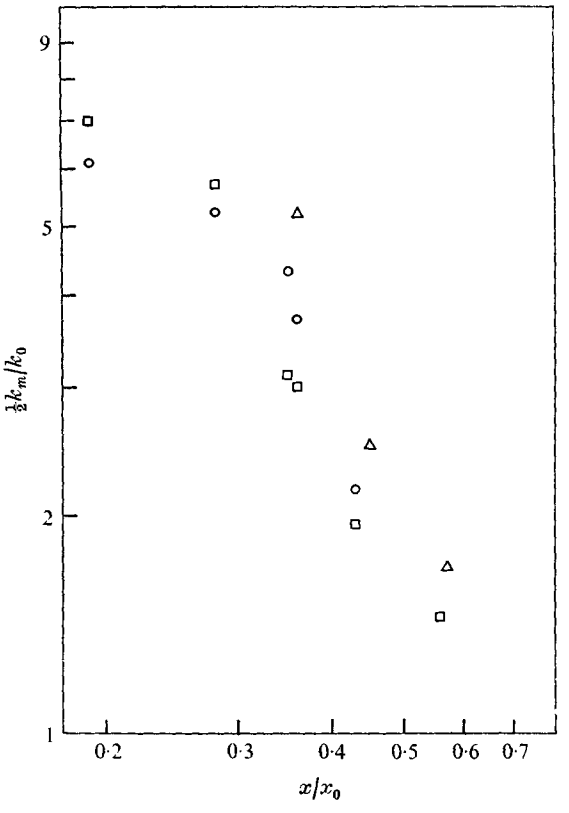

FIGURE 10. Spatial variation of the wavenumber for $\gamma \approx c$. $\sigma/N = 0{\cdot}075$. ○, △, $a_0 = 0{\cdot}2$ cm; □, $a_0 = 0{\cdot}4$ cm.

energy flux. Figure 11 shows that the measured values of the wave amplitude are highest near $-z/cx = 1{\cdot}0$ for each frequency. However, it is not conclusively shown in this figure that the amplitudes peak exactly at this position. The experimental values $(a_m/a_0)^2$ increase sharply towards the critical characteristic; beyond this point, the amplitude ratios then decrease towards the slope. The larger input waves grow more rapidly as the critical characteristic is approached. Other results show that the amplitude ratios increase with decreasing wave frequency at equal values of $-z/cx$.

The theoretical curves for $n = -1$ and $n = -2$ are also shown in figure 11. The theory of I selects $n = -2$ as the lowest non-singular inviscid mode for the experimental conditions tested. The curve for $n = -2$ does not predict the sharp increase in measured amplitudes toward the critical characteristic, nor does it show the decrease in amplitudes at positions between the critical characteristic and the slope ($-z/cx < 1{\cdot}0$).

Results for the probe measurements of wave amplitude when $\gamma \approx c$ are shown in figure 12. The increase in amplitude over the range $0{\cdot}28 < x/x_0 < 0{\cdot}60$ is similar to the increase shown in figure 11 for the same range. However, the maximum

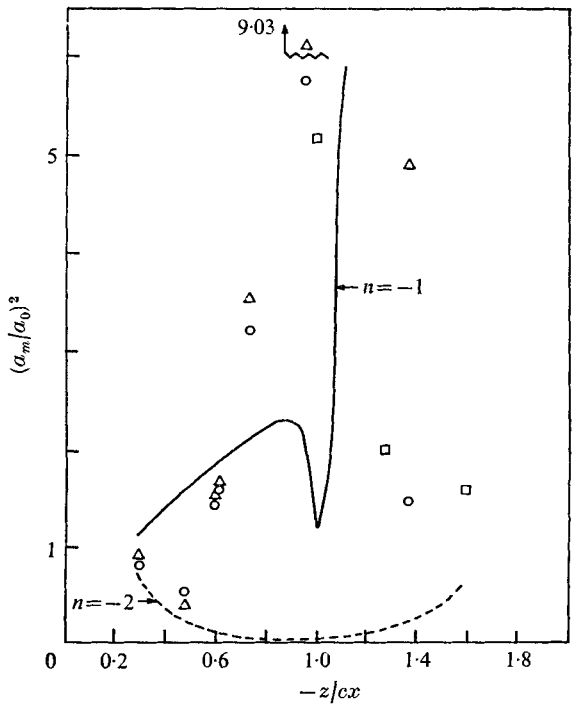

FIGURE 11. Spatial variation of the wave amplitude for $\gamma > c$. $\sigma/N = 0{\cdot}05$. ○, □, $a_0 = 0{\cdot}2$ cm; △, $a_0 = 0{\cdot}4$ cm. The data were taken at a constant value of $-z = 6{\cdot}0$ cm.

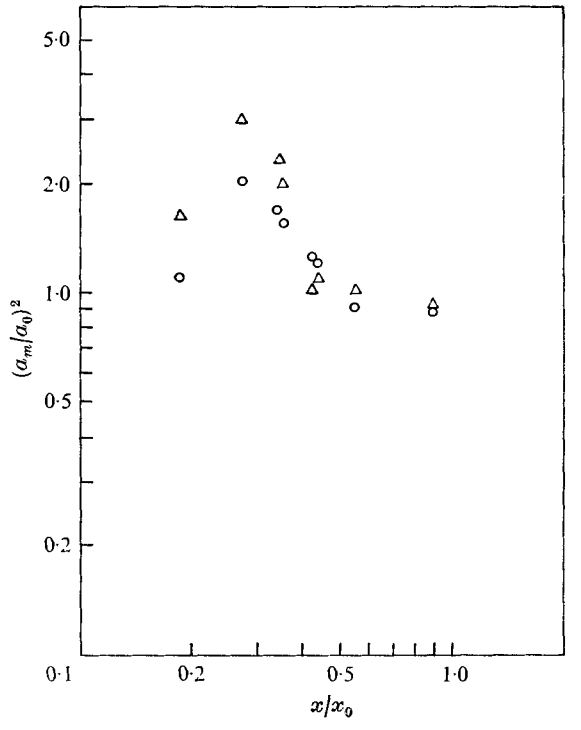

FIGURE 12. Amplitude variation for $\gamma \approx c$. $\sigma/N = 0{\cdot}075$.
○, $a_0 = 0{\cdot}2$ cm; △, $a_0 = 0{\cdot}4$ cm.

amplitude measured for these waves is considerably less than the corresponding value for the supercritical case. Larger viscous dissipation along the slope in the critical case (see below) appears to explain the smaller peak amplitude levels.

In summary, the data indicate that the wave amplitudes generally increase sharply during shoaling over the middle sections of the slope. Peak levels of amplitude were generally found near $-z/cx = 1{\cdot}0$. Peak values of amplitudes for waves of critical frequency are consistently lower than those at lower frequencies. In both cases the wave amplitudes diminish near the slope, but remain larger than the input values. Measurements of amplitude agree qualitatively with the reflexion properties of internal waves from a rigid sloping bottom, but cannot be compared directly to the predictions in I.

4.4. *Boundary activity*: $\gamma = c$ *and* $\gamma > c$

With $\gamma = c$ and with steep slopes (30 and 45°), intense mixing occurs in a zone of waves breaking near the corner similar to that described for the subcritical waves on a 30° slope. For runs with gentler slopes (7 and 15°), each wave, for both the critical and supercritical cases, forms a surge that usually ends with a short run-up. This run-up typically covers much shorter distances than run-up for waves in the subcritical case.

Figure 13 (plate 3) illustrates in a very striking way that the shoaling of internal waves for critical and supercritical cases produces an instability along the slope prior to breaking. Shadowgraphs of the instability illustrated in figure 13 indicate that a line of regularly spaced vortices forms near the bottom. These vortices grow and decay over each half-cycle as they oscillate along the slope at the frequency of the input waves. During downslope particle motion in the waves, the vortices 'flatten', indicating that they form only during the upslope movement of the water particles. The circulations of adjacent vortices have the same sense and the axis of each vortex is oriented approximately normal to the side walls of the tank. The maximum distance observed between the core of adjacent vortices was about 2 cm. Unlike the vortices which form and propagate upslope beneath the shoaling subcritical waves prior to violent breaking, these vortices ($\gamma = c$) retain their cyclic growth and decay pattern for the duration of the input wave motion. Their regular spacing is much shorter than the wavelength of the input waves, and presumably is related to the boundary-layer scale.

The onset of vortex activity for any particular run normally occurs within 10–20 wave periods after the arrival of the first wave motion at the corner region of the slope. The initial vortex generally appears somewhere along the middle section of the slope, and the instability spreads gradually towards the corners. The initiation of vortex activity was observed as a function of input frequency. These results indicate that (i) the vortices occur earliest (in time measured from the start of the wave maker) for $\gamma = c$, (ii) for small enough $c < \gamma$, no vortices appear, and (iii) there is a small range of $\gamma < c$ (subcritical) when vortices do appear though precise values are hard to specify.

The diameters of the vortices were difficult to measure accurately from the shadowgraph images because of the constant process of either growth or decay during each half-cycle. From data taken from various photographs, the size of

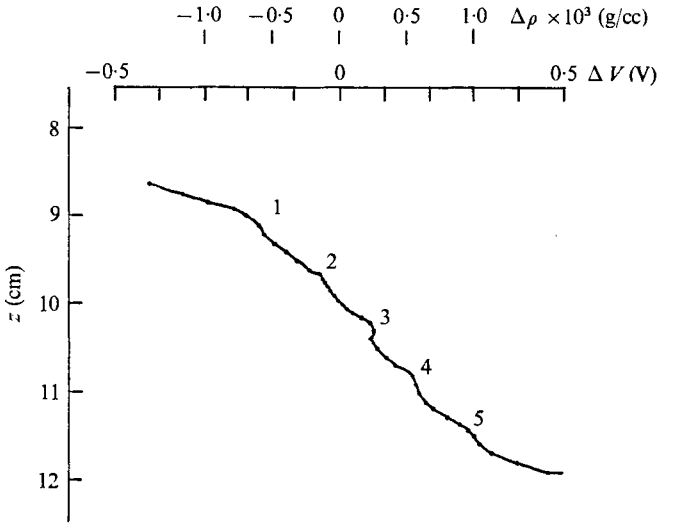

FIGURE 14. A density profile taken through the streamers of figure 13, showing the microstructure that is formed along the slope. Numbers are adjacent to the nearby homogeneous streamers that are formed by mixing in the vortex cells.

the vortex diameters is largest for $c \sim \gamma$ and generally decreases for lower and higher values of c.

Shortly after the formation of the line of vortices, thin streamers or wisps appear near the cusp of each vortex and penetrate into the interior of the fluid (note the thin lighter bands that alternate with the darker bands in figure 13). Qualitatively, it appears that fluid of slightly different densities from vertical levels adjacent to each vortex cell is mixed in the cell and returns to the interior as a thin streamer at a new equilibrium level. The result of this process is alternate layers of thin nearly homogeneous streamers and thicker linearly stratified laminae.

Shadowgraph images of the thin horizontal streamers usually intensify with time if the wave motion continues. The shadowgraph images of the streamers are sharply outlined near the vortices, but within short horizontal distances from the slope (of order 2–4 cm) the images weaken, although they can be detected out to distances of 20 cm horizontally from the bottom.

Several conductivity probe traverses through short vertical sections (3 and 4 cm) were made in order to detect changes in the linear density–depth profiles that might be associated with the streamers. Figure 14 shows the measured density structure for a typical vertical traverse of a probe after the formation of the streamers. Small-scale irregularities which can be described as 'microstructure' are typical of these profiles. Sharp changes in density at the edges of the nearly homogeneous streamers are apparent in the shadowgraphs and conductivity measurements. The density gradients are not homogeneous within the laminae, but are approximately equal to the overall mean gradient.

The net movements of neutrally buoyant particles in the streamers and in the intervening laminae were observed for several runs. The typical net motion was away from the slope in the streamers and towards the slope in the laminae with magnitude of about 0·2 mm/s.

5. Summary

The linear theory of internal waves of the fundamental mode travelling over a uniform slope is in quite good agreement with experimental results in the subcritical case, sufficiently far from the corner region. Breakdown of the waves occurs through strong dissipation along the slope, and especially at high frequencies, through a breaking mechanism. At lower frequencies, the waves have a tendency to 'surge' along the bottom with large viscous losses.

In the case of a supercritical slope, no theory was actually tested, but the wave field is clearly inhomogeneous with nonlinear processes important in the vicinity of the critical characteristic. These waves tend not to break, but to dissipate through laminar processes.

At the critical frequency, where the direction of energy flux in the wave is parallel to the slope, the boundary layer at the bottom is unstable, generating periodic vortices which mix fluid locally. This mixed fluid propagates into the interior of the fluid and is apparent as a density 'microstructure'. Breaking that is considerably less energetic than that for the subcritical case also occurs near the corner when $\gamma \approx c$; its intensity diminishes with $\gamma > c$.

Supported by the Office of Naval Research under contracts N00014-67-A-0204-0047, -0048. The glass tank was provided by the Educational Development Center of Newton, Massachusetts. Dr Seelye Martin made several helpful suggestions concerning the experimental techniques.

REFERENCES

BAINES, P. G. 1971 The reflexion of internal/inertial waves from bumpy surfaces. Part 2. Split reflexion and diffraction. *J. Fluid Mech.* **49**, 113–131.

BEARDSLEY, R. C. 1970 An experimental study of inertial waves in a closed cone. *Studies in Appl. Math.* **49**, 187–196.

CACCHIONE, D. 1970 Experimental study of internal waves on a slope. Ph.D. thesis, p. 226, M.I.T./W.H.O.I.

CACCHIONE, D. & SOUTHARD, J. B. 1974 Incipient sediment movement by shoaling internal gravity waves. *J. Geophys. Res.* **79**, 2237–2242.

EMERY, K. O. & GUNNERSON, C. G. 1973 Internal swash and surf. *Proc. Nat. Acad. Sci.* **70**, 2379–2380.

GREENSPAN, H. P. 1969 On the inviscid theory of rotating fluids. *Studies in Appl. Math.* **48**, 19–28.

HART, J. E. 1971 A possible mechanism for boundary layer mixing and layer formation in a stratified fluid. *J. Phys. Oceanog.* **1**, 258–262.

HOGG, N. G. 1971 Long shore current generation by obliquely incident internal waves. *Geophys. Fluid Dyn.* **2**, 361–376.

HURLEY, P. M. 1970 Internal waves in a wedge-shaped region. *J. Fluid Mech.* **43**, 97–120.

KELLER, J. B. & MOW, V. C. 1969 Internal wave propagation in an inhomogeneous fluid of non-uniform depth. *J. Fluid Mech.* **38**, 365–374.

LAMB, H. 1932 *Hydrodynamics*. Cambridge University Press.

MAGAARD, L. 1962 Zur berechung interner Wellen im meeresraumen mit nichtebenen Böden dei einer speziellen Dichteverteilung. *Kiel Meeresforsch.* **18**, 161–183.

MOWBRAY, D. E. 1967 The use of schlieren and shadowgraph techniques in the study of flow patterns in density stratified fluids. *J. Fluid Mech.* **27**, 595–608.

OSTER, G. 1965 Density gradients. *Sci. Am.* **213**, 70–76.

PHILLIPS, O. M. 1966 *Dynamics of the Upper Ocean.* Cambridge University Press.

PHILLIPS, O. M. 1970 On flows induced by diffusion in a stably stratified fluid. *Deep-Sea Res.* **17**, 435–443.

ROBINSON, R. M. 1970 The effects of a corner on a propagating internal gravity wave. *J. Fluid Mech.* **42**, 257–267.

SANDSTROM, H. 1966 The importance of topography in generation and properties of internal waves. Ph.D. thesis, University of California, San Diego.

THORPE, S. A. 1966 Internal gravity waves. Ph.D. thesis, University of Cambridge.

TURNER, J. S. 1973 *Buoyancy Effects in Fluids.* Cambridge University Press.

WUNSCH, C. 1969 Progressive internal waves on slopes. *J. Fluid Mech.* **35**, 131–144.

WUNSCH, C. 1970 An oceanic boundary mixing. *Deep-Sea Res.* **17**, 293–301.

WUNSCH, C. 1971 Note on some Reynolds stress effects of internal waves on slopes. *Deep-Sea Res.* **16**, 583–591.

WUNSCH, C. & HENDRY, R. 1972 Array measurements of the bottom boundary layer and the internal wave field on the continental slope. *Geophys. Fluid Dyn.* **4**, 101–145.

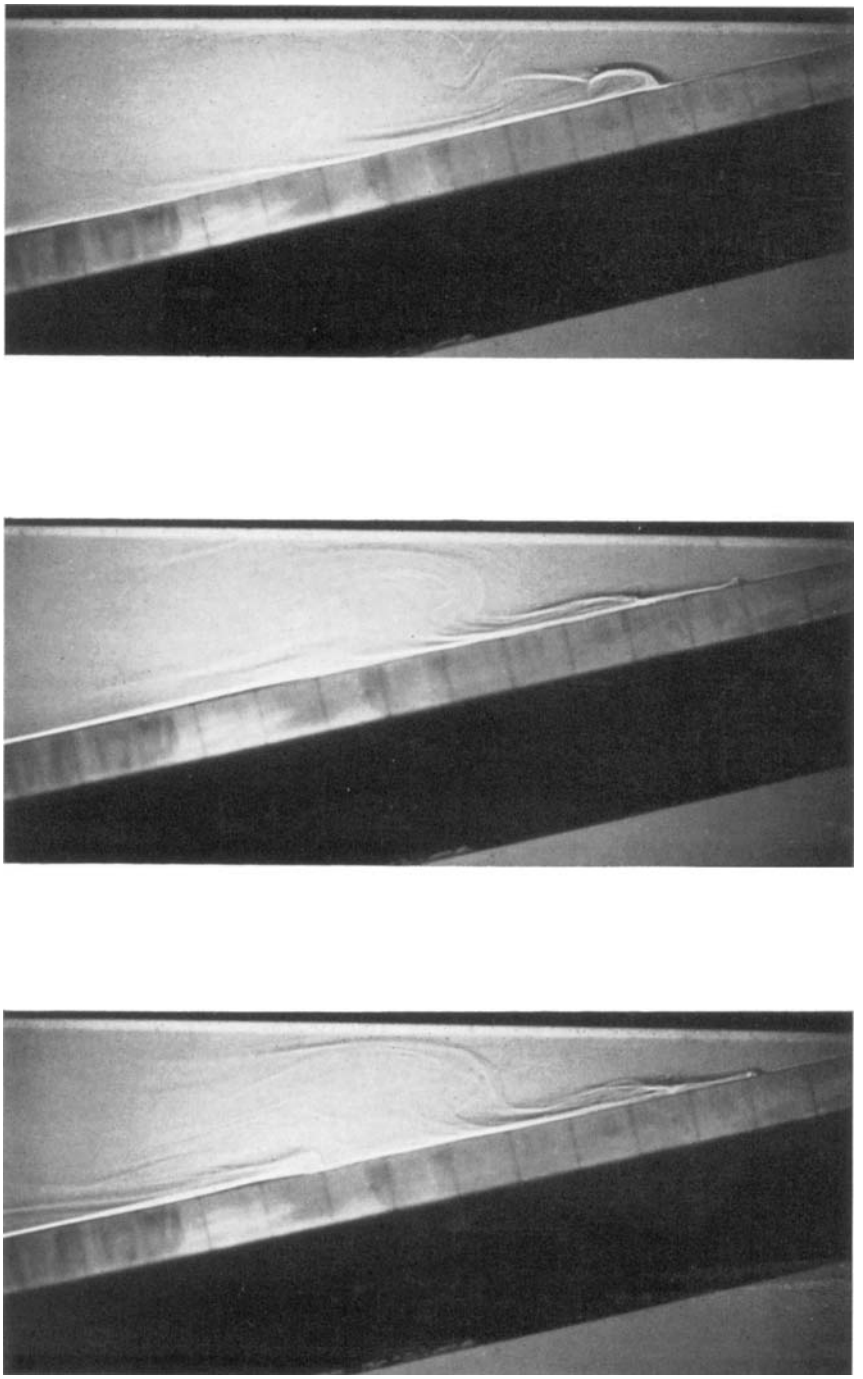

FIGURE 6. Sequence of shadowgraph pictures showing breakdown of a low frequency wave with $\gamma < c$, at various times. Note the formation of a bore-like phenomenon along the slope. In this case $a_0 = 0{\cdot}4$ cm; $\sigma = 0{\cdot}4$ s^{-1}. Distance between heavy dark lines along slope is 2 cm; undisturbed free surface is at the intersection of the dark and light regions at the top of the photographs.

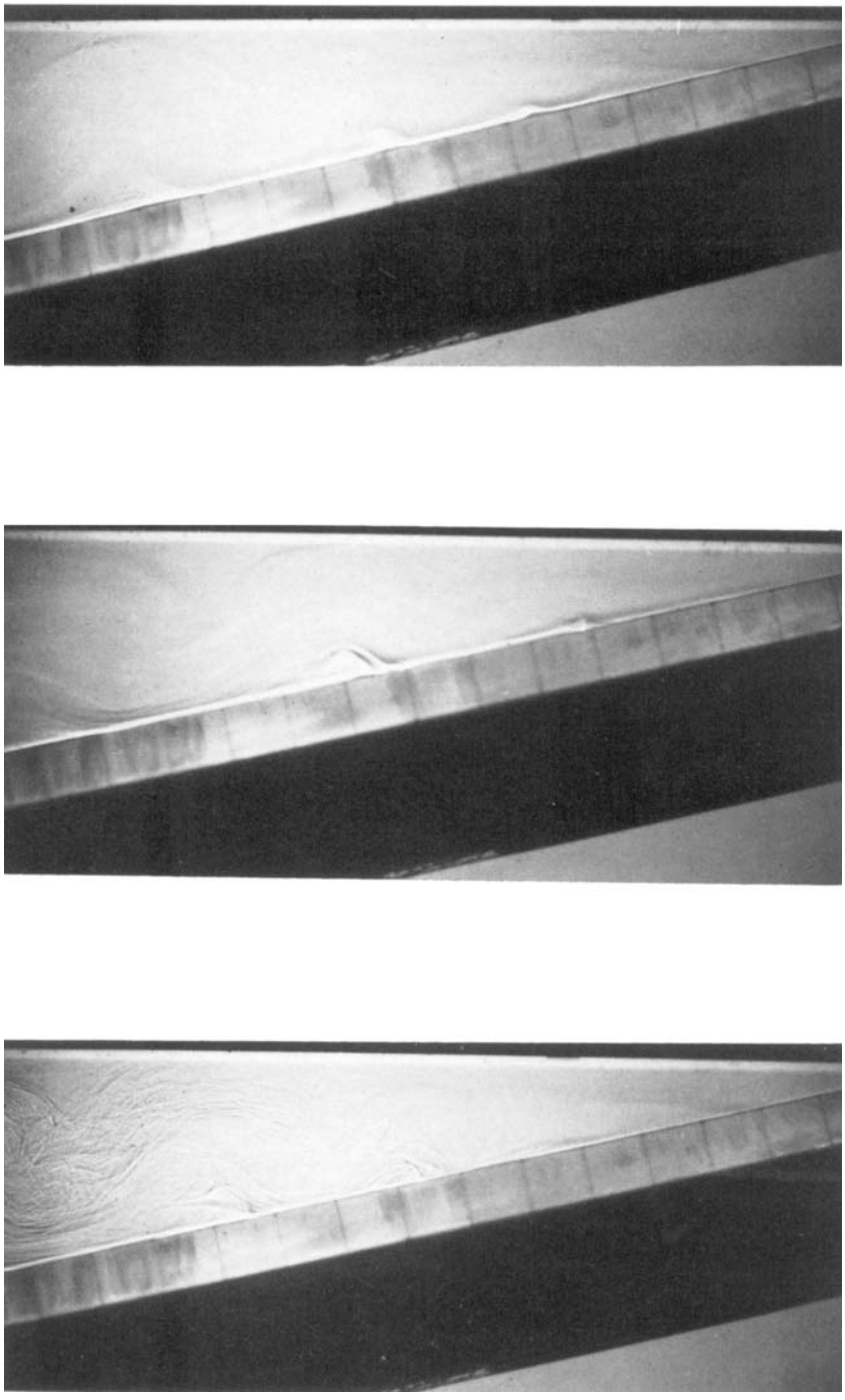

FIGURE 7. Sequence of shadowgraph pictures showing breakdown of a high frequency wave with $\gamma < c$, at various times. A multiple set of crests forms along the slope. In this case $a_0 = 0{\cdot}4$ cm; $\sigma = 0{\cdot}75$ s^{-1}.

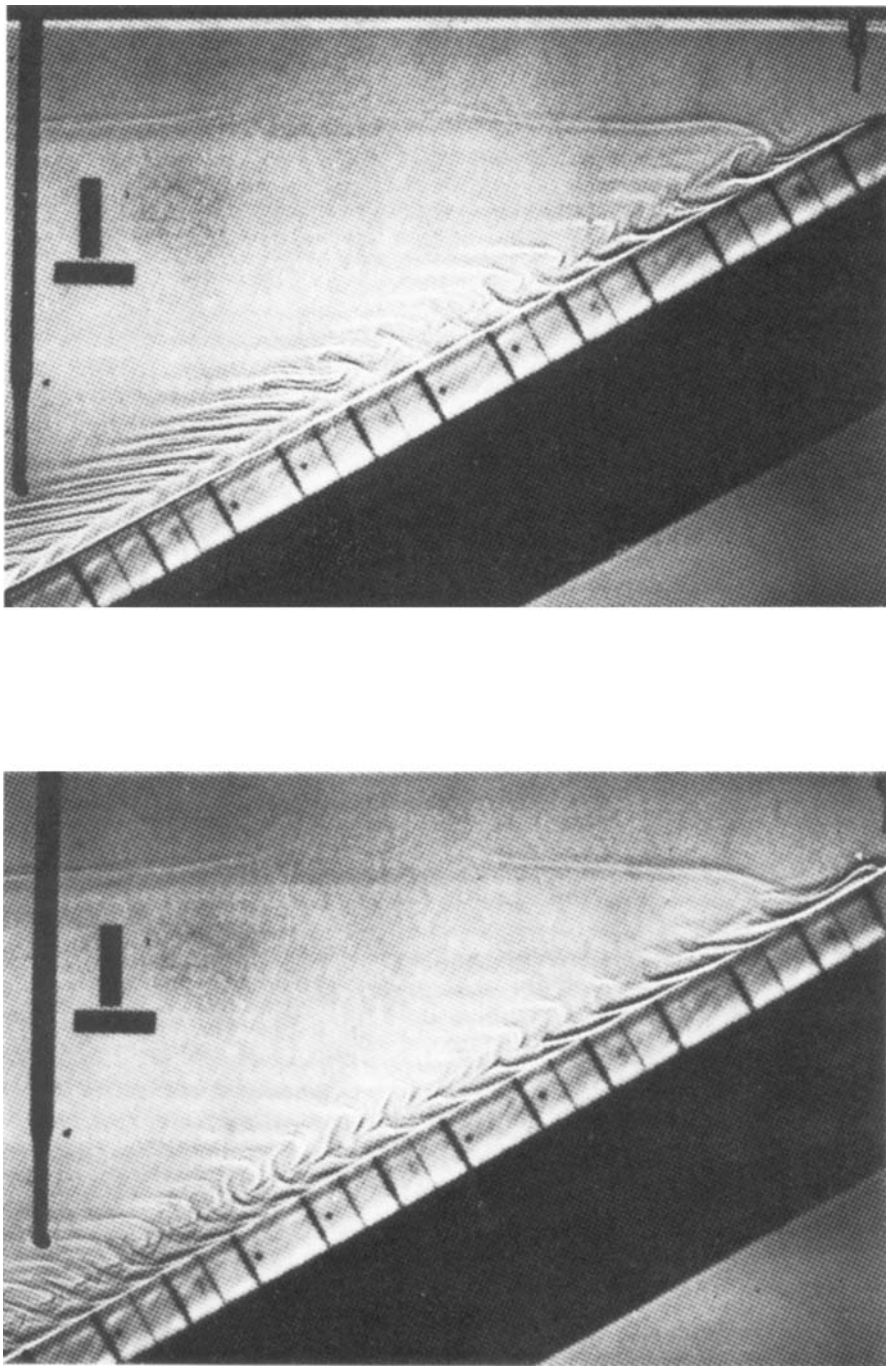

FIGURE 13. Shadowgraph picture of the instability in the bottom boundary layer in the critical case for two phases of the incident waves. The thin streamers (lighter zones in the shadowgraph) represent fluid that has been mixed in the boundary layer and is penetrating into the interior of the fluid. The long vertical object on the left in the pictures is a conductivity probe. The spacing between heavy black lines along the slope is 2 cm. $a_0 = 0{\cdot}2$ cm; $\sigma = 0{\cdot}48\ \mathrm{s}^{-1}$.

CACCHIONE AND WUNSCH